


RESEARCH ARTICLE | FEBRUARY 21 2017

Optically controllable nanobreaking of metallic nanowires

Lina Zhou; Jinsheng Lu ; Hangbo Yang; Si Luo; Wei Wang; Jun Lv; Min Qiu; Qiang Li



Appl. Phys. Lett. 110, 081101 (2017)

<https://doi.org/10.1063/1.4976947>



CrossMark

500 kHz or 8.5 GHz?
And all the ranges in between.

Lock-in Amplifiers for your periodic signal measurements



Find out more



Optically controllable nanobreaking of metallic nanowires

Lina Zhou, Jinsheng Lu, Hangbo Yang, Si Luo, Wei Wang, Jun Lv, Min Qiu, and Qiang Li^{a)}

State Key Laboratory of Modern Optical Instrumentation, College of Optical Science and Engineering, Zhejiang University, Hangzhou 310027, China

(Received 13 December 2016; accepted 7 February 2017; published online 21 February 2017)

Nanobreaking of nanowires has shown its necessity for manufacturing integrated nanodevices as nanojoining does. In this letter, we develop a method for breaking gold pentagonal nanowires by taking advantage of the photothermal effect with a 532 nm continuous-wave (CW) laser. The critical power required for nanobreaking is much lower for perpendicular polarization than that for parallel polarization. By controlling the polarization and the power of the irradiation light for nanobreaking, the nanowires can be cut into segments with gap widths ranging from dozens of nanometers to several micrometers. This CW light-induced single point nanobreaking of metallic nanowires provides a highly useful and promising method in constructing nanosystems.

Published by AIP Publishing. [<http://dx.doi.org/10.1063/1.4976947>]

Nanowires (NWs) are regarded as one of the essential building blocks for constructing complex nanostructures.^{1–4} So far, nanojoining of NWs has shown its necessity in manufacturing integrated nanodevices.^{5–15} Similarly, nanobreaking of NWs, which can be described as formation of a gap from one NW, also plays a vital role in integrated nanodevices.^{16,17} On the one hand, nanobreaking of NWs provides a convenient method for acquiring NWs with desired lengths in optical and electronic circuits;¹⁸ on the other hand, it provides an opportunity of forming desired gaps for nanometer- or micrometer-spaced electrodes used in sensors,¹⁹ transistors,²⁰ molecular electronics,²¹ etc. The nanobreaking of NWs thereby enables miniaturization and integration of mechanical, photonic, and electronic devices.

So far, several methods have been implemented to achieve nanobreaking of NWs. (i) Electromigration by applying current has been widely used for nanobreaking of NWs.^{22–26} This method shows superiority in mass production through a feedback-controlled processing step.²⁶ However, the breaking positions of the NWs and shapes of the new ends are uncontrollable. (ii) Mechanical nanobreaking methods including bending, stretching, and direct scratching by applying external force have been introduced in fabricating transistor architectures.^{27–29} The breaking position is also uncontrollable and the inevitable contact with the sample could degrade its mechanical performance. (iii) Focused electron/ion beam-based methods have been proposed in nanobreaking for construction of integrated circuits.^{30,31} This method possesses a high degree of control over the formed gap size. However, the cost of this method is relatively high and contamination (such as gallium ions) is inevitably brought in. (iv) Heat induced nanobreaking caused by Rayleigh instability has been introduced in mass production of optical waveguides.³² During the thermal annealing, the NWs undergo a morphological instability and this method is only effective for NWs with small diameters (<50 nm). The light induced localized thermal effect provides an alternative for nanobreaking of NWs. With a

sufficient amount of light power focused onto the metallic NW, the light induced photothermal effect can significantly increase the surface temperature of the NW until it reaches the threshold of melting,^{33–43} resulting in the breaking of the NW. Also, the photothermal effect of the metal NW depending on laser polarization direction has been observed.¹³ Therefore, light induced nanobreaking of NWs provides an ideal candidate for constructing nanostructures.

In this paper, we report an optically controllable method for nanobreaking of metallic NWs based on the photothermal effect induced by continuous-wave (CW) laser. First, the morphological changes of the NWs from partial melting to complete breaking after irradiation are investigated. The measured critical power for nanobreaking at perpendicular polarization (with respect to the NWs) is much lower than that at parallel polarization and the physics behind is unveiled based on electromagnetic and thermal simulations. Then, size control over the gap size with power of the irradiation light is explored. Finally, potential applications of this optically controllable nanobreaking are discussed. The CW light-induced nanobreaking of NWs presented here offers several distinct advantages. (i) The position of nanobreaking, which is determined by the irradiation position of focused laser beam, is highly controllable. (ii) The non-contact handling method provides unprecedented spatial manipulation flexibility for nanobreaking. (iii) The use of CW rather than pulsed laser reduces the operating cost. Therefore, this light-induced single-point nanobreaking provides a highly useful and promising method in constructing nanosystems.

A schematic of the experimental setup is illustrated in Fig. 1. The output power from a 532 nm CW laser is controlled by the first Glan-Taylor polarizer (GTP). The output beam is linearly polarized after passing through the second GTP. A half-wave plate is used to obtain parallel or perpendicular polarizations with respect to the NWs. A mechanical shutter is utilized to control the laser irradiation time to be 2 ms, which is well above the time scale (typically ~100 ps) for thermal diffusion in nanoscale systems.^{6,44} The laser beam is transmitted through a beam splitter and focused by a 100× objective lens onto the sample. The numerical aperture

^{a)}Email: qiangli@zju.edu.cn

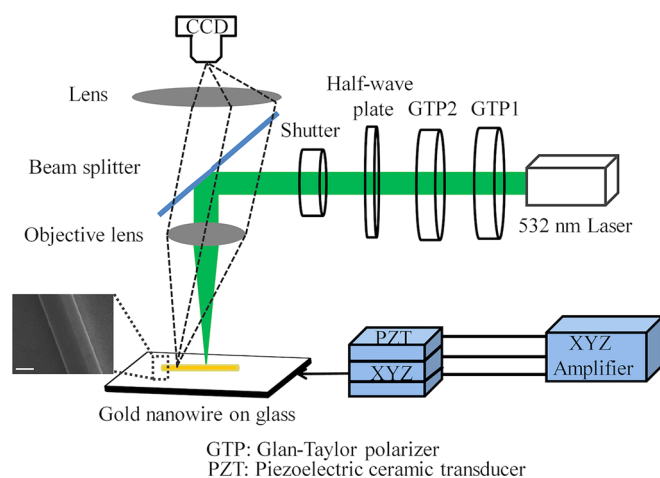


FIG. 1. A schematic of the experimental setup. Inset is the SEM image of the gold pentagonal NW (400 nm in diameter). Inset scale bar is 200 nm.

of the objective lens is 0.5. The diameter of the laser spot is about 460 nm (calculated by $1/e$ base). A three-dimensional positioning stage attached to a piezoelectric ceramic transducer (PZT) is adopted to control the position of the sample. A CCD mounted on the optical microscope is utilized to observe and record the nanobreaking. The gold NWs with pentagonal cross-sections are synthesized by modifying the molar ratio of aniline and gold from 2:1 to 73:36 in the wet-chemical approach previously used for synthesizing gold nanoplates.⁴⁵ Diameters of the synthesized gold NWs range from 180 nm to 360 nm with lengths between 20 μm and 30 μm .

Morphological changes of the NW with increased irradiation power are first investigated. The diameter of the NW used here is about 300 nm. The irradiation polarization is parallel to the NW and the irradiation time is 2 ms. Irradiations aiming at three positions quartering the NW (schematically denoted by “B”, “C”, and “D” in Fig. 2(a)) are implemented. The three irradiation spots are spaced far enough so that the morphological change caused by the former irradiation does not affect the following nanobreaking. The corresponding irradiation power used in the experiment is 39 mW, 40 mW, and 42 mW, and the corresponding laser fluence is 47 mJ/cm^2 , 48 mJ/cm^2 , and 51 mJ/cm^2 , respectively. With an irradiation power of 39 mW (47 mJ/cm^2),

surface melting of the NW occurs apparently at the irradiation position, producing a sphere-like structure wrapping the original NW; however, no complete breaking can be observed (Fig. 2(b)). With an irradiation power of 40 mW (48 mJ/cm^2), the gold NW breaks into two segments at the irradiation position, forming a 58-nm gap (Fig. 2(c)). A nanosphere is also formed close to one end after the nanobreaking. With an irradiation power of 42 mW (51 mJ/cm^2), complete nanobreaking with a much wider gap (648 nm) is achieved. A relatively round nanosphere is formed right at the end of the NW after the nanobreaking. Besides the power used in Figs. 2(b)–2(d) (39 mW, 40 mW, and 42 mW), we also irradiate the 300-nm-diameter NW with the power of 37 mW and 43 mW (shown in Fig. S1 (supplementary material)). At 37 mW irradiation power (lower than the 39 mW critical power), the NW will not melt no matter how long the irradiation time is. A wider gap (2166 nm) will form when the irradiation power is increased to 43 mW at parallel polarization. In addition, the relationship between the irradiation power and irradiation time is also investigated. When the irradiation power is far below the critical power, a further increase in irradiation time will not contribute to the nanobreaking of NWs. There is no morphological change at irradiation power below 37 mW no matter how long the irradiation time is. When the irradiation power is slightly below the critical power, increasing irradiation time can facilitate the nanobreaking (shown in Fig. S2 (supplementary material)). The morphological changes of the NWs with increased irradiation power explicitly indicate that a critical power is required for nanobreaking and critical power for nanobreaking might be lower with longer irradiation time.

The critical power for optical induced nanobreaking of NWs with different diameters (200–300 nm) is then measured at parallel and perpendicular polarizations (Fig. 3), which ranges from 35 to 45 mW (42 to 54 mJ/cm^2) at perpendicular polarization and from 25 to 35 mW (30 to 42 mJ/cm^2) at parallel polarization. No obvious dependence of the critical power for nanobreaking on the NW diameter can be identified here. For the same NW, the critical power for nanobreaking at perpendicular polarization is lower than that at parallel polarization by around 10 mW (12 mJ/cm^2), demonstrating that the perpendicular polarization is more energy-efficient for the breaking of NWs. As a typical example, SEM images of a 300-nm-diameter NW after being

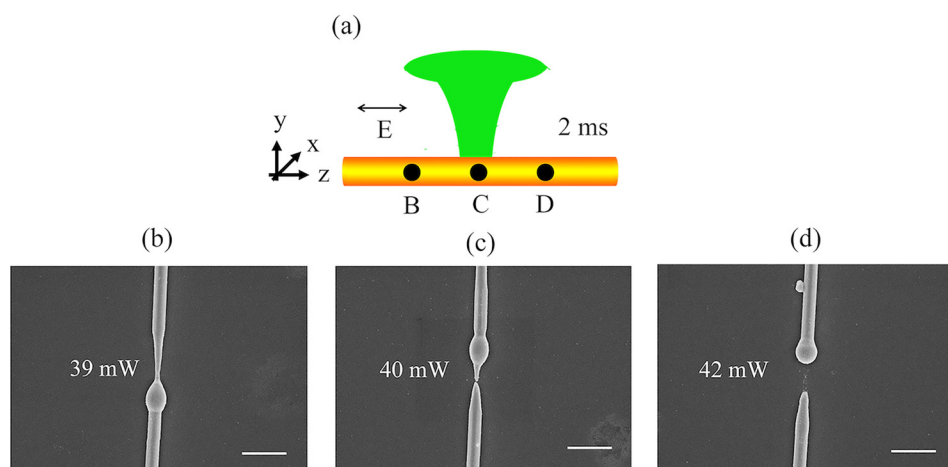


FIG. 2. Morphological changes of a 300-nm-diameter gold NW after light irradiation with different powers at parallel polarization. (a) A schematic illustration of a focused Gaussian light irradiated on different positions. The irradiation power (laser fluence) is (b) 39 mW (47 mJ/cm^2), (c) 40 mW (48 mJ/cm^2), and (d) 42 mW (51 mJ/cm^2) for positions “B”, “C”, and “D”, respectively. The formed gap widths are (b) 0 nm, (c) 58 nm, and (d) 648 nm. Inset scale bars are 1 μm .

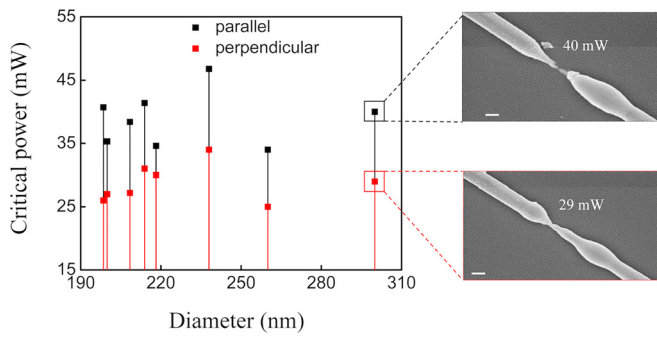


FIG. 3. The measured critical power required for nanobreaking for different NW diameters at parallel (black dots) and perpendicular polarizations (red dots). The SEM images of the 300-nm-diameter NW after nanobreaking at critical power (40 mW (48 mJ/cm²) and 29 mW (35 mJ/cm²) for parallel and perpendicular polarizations, respectively). Inset scale bars are 200 nm.

irradiated by corresponding critical power at parallel and perpendicular polarizations are provided (Fig. 3). At parallel polarization, the NW almost breaks with the irradiation power of 40 mW (48 mJ/cm²), while at perpendicular polarization the nanobreaking occurs at the irradiation power of 29 mW (35 mJ/cm²).

To unveil the physics behind the differences in the critical power for polarization dependent nanobreaking between the two polarizations, electromagnetic fields and temperature distributions are calculated with the commercial finite element method based on COMSOL multiphysics. In the simulations, the diameter and the length of the pentagonal gold NW are 300 nm and 20 μ m, respectively. The irradiation power is fixed at 40 mW (48 mJ/cm²). Here, we assume that the NW is not broken and only consider the steady-state case since the irradiation time in experiments (~ 2 ms) is much longer than thermal response time (on the order of nanosecond). The heat source per unit volume (also termed as “heat power density”) is related to the electric field E by $Q = \frac{1}{2} \epsilon_0 \omega \text{Im}(\epsilon_r) |E|^2$, where ϵ_0 and ϵ_r are vacuum permittivity and relative permittivity of gold (8.85×10^{-12} F/m and $-4.72 + 2.39i$, respectively); ω is the frequency of the light. With heat source distribution Q , the spatial temperature (T) distribution can then be resolved based on the steady-state heat transfer equation $k \nabla^2 T + Q = 0$, where k is the thermal conductivity (317 W/(m·K) for bulk gold).⁴⁴ It is worth mentioning that the conduction heat transfer through the substrate is also taken into consideration in the simulations. The exact thermal parameters (melting point and thermal conductivity k) for NWs are unknown and they are much lower than those for bulk gold. The results of the simulations are used to qualitatively determine which polarization is more effective for nanobreaking in terms of the temperature rise. The two polarizations excite two different propagating plasmonic waveguide modes in the gold NWs (Figs. 4(a) and 4(b)), agreeing with previous studies on the modes in metallic NWs.⁵ For the plasmonic mode excited at parallel polarization, the electric field is predominantly confined at the top corner of the pentagonal cross-section (Fig. 4(a)). The calculated effective refractive index and propagation length of this plasmonic mode are 1.20 and 0.32 μ m, respectively. In comparison, the electric field of the plasmonic mode excited at perpendicular polarization mainly concentrates around the

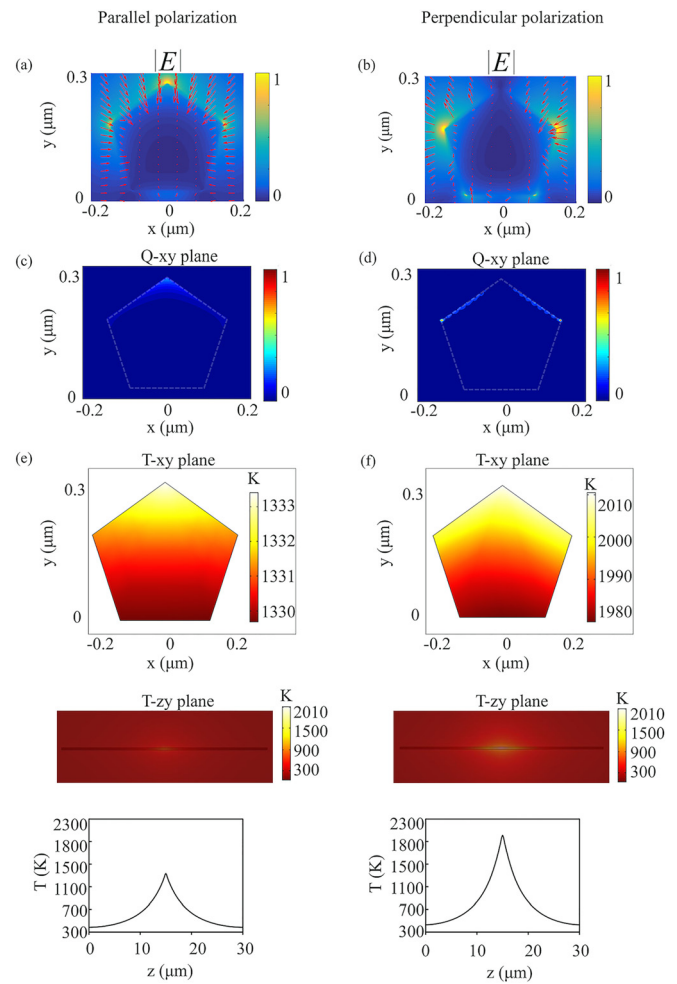


FIG. 4. Simulated electromagnetic fields and temperature distributions for a NW (300 nm in diameter and 30 μ m in length) at parallel (left column) and perpendicular polarizations (right column). (a) and (b) Electric field intensity of the two excited plasmonic modes in the pentagonal cross-section of the NW ($z=0$). (c) and (d) Heat power density Q in the pentagonal cross-section of the NW. (e) and (f) Steady-state temperature distributions in the cross-sections of the NW ($z=0$ and $x=0$) and temperature distributions as a function of distance along the NW.

two lower corners of the pentagonal cross-section (Fig. 4(b)). This plasmonic mode presents an effective refractive index of 1.04 and a propagation length of 0.36 μ m. Therefore, the difference in the propagation losses of the two plasmonic modes excited by the two polarizations is not significant. However, the generated heat power density at perpendicular polarization is greater than that at parallel polarization (Figs. 4(c) and 4(d)). This is because the excitation of the plasmonic mode at perpendicular polarization (0.40) is much more efficient than that at parallel polarization (0.21). Consequently, a higher portion of light impinging on the NW is converted into heat within the NW at perpendicular polarization. From the steady-state temperature distributions in the cross-sections ($z=0$, $x=0$) of the NW (Figs. 4(e) and 4(f)), the peak temperatures are 1433 K and 2834 K after irradiation at parallel and perpendicular polarizations, respectively. It should be noted that the peak temperatures at both polarizations are higher than the gold melting point (1020 K in Ref. 46) and the peak temperature at perpendicular polarization is far higher than that at parallel polarization. Therefore, the critical power for nanobreaking

is much lower at perpendicular polarization than that at parallel polarization.

When the irradiation power is above the critical power, the formed gap sizes are strongly related to the irradiation power and the NW diameter. To control the nanobreaking of the gold NWs, dependence of gap size after nanobreaking on light power and NW diameter is further studied. Figures 5(a) and 5(b) show the gap sizes after nanobreaking with different irradiation powers higher than the critical power and NW diameters (182–322 nm) at two polarizations (parallel and perpendicular). Three different end configurations (corresponding images are shown in insets) are generated after nanobreaking: double nanospheres, single nanosphere, and no nanosphere, which are represented by asterisk, square, and triangle in graphs of Fig. 5, respectively. For consecutive nanobreaking in the same NW, the irradiation positions are $>5\mu\text{m}$ apart in order to minimize the effect of the NW length on the nanobreaking. While the dependence of the gap size on the NW diameter with the same power is not so obvious, the gap size generally increases with the increasing irradiation power when irradiating on the same NW. The formed nanogap sizes for parallel polarization are generally larger than those for perpendicular polarization. The gap size is related to the gap resonance at different irradiation

polarizations. When the irradiation power is above the critical power for nanobreaking, the NW breaks into two segments and a nanogap is then formed on a submillisecond time scale. The irradiation then excites the gap-mode resonance. For the gap-mode resonance, the coupling efficiency and corresponding field enhancement for parallel polarization are much stronger than those for perpendicular polarization. Therefore, the formed gap size is larger for parallel polarization than that for perpendicular polarization. There is usually a single nanosphere formed at the end of the NW after nanobreaking (Fig. 5). The occurrence of double nanospheres and no nanosphere is rare. Also, the end configurations after nanobreaking are uncontrollable. Therefore, the NWs can be cut into required lengths and desired nanogap sizes can be obtained after nanobreaking with suitable power and polarization.

In conclusion, we have developed a convenient method for breaking metallic NWs based on the photothermal effect with a CW laser. The critical power required for nanobreaking is much lower at perpendicular polarization than that at parallel polarization, which can be attributed to the higher excitation efficiency of the plasmonic waveguide mode for perpendicular polarization. Through controlling the irradiation power and polarization, desired sizes of gaps ranging from dozens of nanometers to several micrometers can be achieved. Through combination with nanowelding,^{10,40} this light-induced non-contact and contamination-free nanobreaking method can be potentially used in building mechanical, photonic, and electronic nano-devices and nano-systems.

See [supplementary material](#) for other power values used to irradiate 300-nm NW at parallel polarization and influences of irradiation time on critical power for 285-nm NW at perpendicular polarization.

This work was supported by the National Natural Science Foundation of China (Grant Nos. 61425023, 61575177, and 61235007).

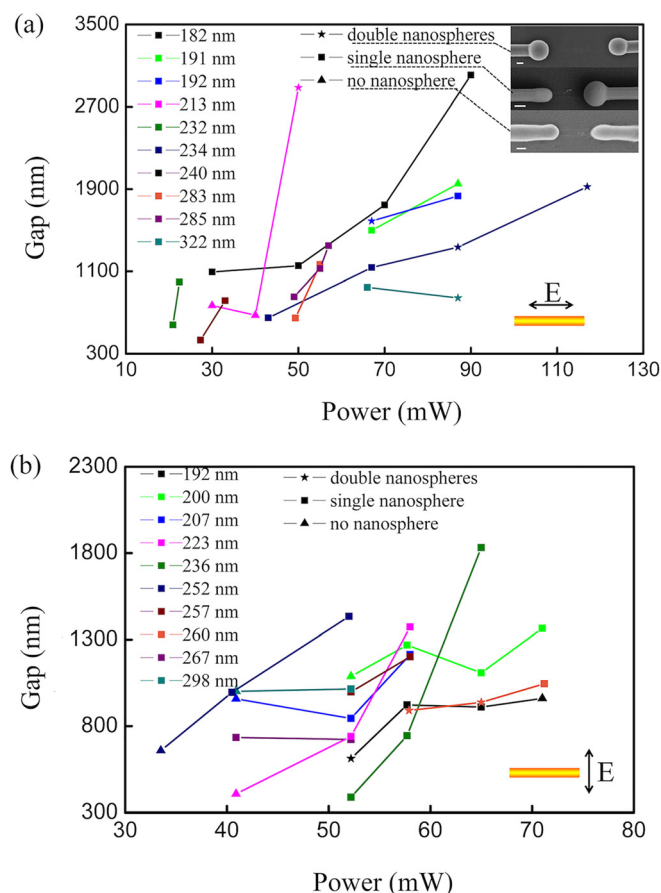


FIG. 5. Measured gap widths for different NW diameters and different irradiation powers (above the critical power for nanobreaking) at (a) parallel and (b) perpendicular polarizations. Insets show the SEM images of three different end configurations generated after nanobreaking including double nanospheres, single nanosphere, and no nanosphere, which are represented by asterisk, square, and triangle in graphs, respectively. Inset scale bars are 200 nm.

- ¹R. Yan, D. Gargas, and P. Yang, *Nat. Photonics* **3**, 569 (2009).
- ²W. Wang, Q. Yang, F. Fan, H. Xu, and Z. Wang, *Nano Lett.* **11**, 1603 (2011).
- ³H. Wei, Z. Li, X. Tian, Z. Wang, F. Cong, N. Liu, and S. Zhang, *Nano Lett.* **11**, 471 (2011).
- ⁴Q. Li and M. Qiu, *Opt. Express* **21**, 8587 (2013).
- ⁵H. Yang, M. Qiu, and Q. Li, *Laser Photonics Rev.* **10**, 278 (2016).
- ⁶L. Liu, P. Peng, A. Hu, G. Zou, W. W. Duley, and Y. N. Zhou, *Appl. Phys. Lett.* **102**, 073107 (2013).
- ⁷Y. Peng, T. Cullis, and B. Inkson, *Nano Lett.* **9**, 91 (2009).
- ⁸E. C. Garnett, W. Cai, J. J. Cha, F. Mahmood, S. T. Connor, M. G. Christoforo, Y. Cui, M. D. McGehee, and M. L. Brongersma, *Nat. Mater.* **11**, 241 (2012).
- ⁹Y. Fang, Z. Li, Y. Huang, S. Zhang, P. Nordlander, N. J. Halas, and H. Xu, *Nano Lett.* **10**, 1950 (2010).
- ¹⁰Q. Li, G. Liu, H. Yang, W. Wang, S. Luo, S. Dai, and M. Qiu, *Appl. Phys. Lett.* **108**, 193101 (2016).
- ¹¹C. F. Guo, Y. Lan, T. Sun, and Z. Ren, *Nano Energy* **8**, 110 (2014).
- ¹²S. Coskun, E. S. Ates, and H. E. Unalan, *Nanotechnology* **24**, 125202 (2013).
- ¹³S. Han, S. Hong, J. Ham, J. Yeo, J. Lee, B. Kang, P. Lee, J. Kwon, S. S. Lee, M. Y. Yang, and S. H. Ko, *Adv. Mater.* **26**, 5808 (2014).
- ¹⁴A. T. Bellew, H. G. Manning, C. Gomes da Rocha, M. S. Ferreira, and J. J. Boland, *ACS Nano* **9**, 11422 (2015).
- ¹⁵Q. Nian, M. Saei, Y. Xu, G. Sabyasachi, B. Deng, Y. P. Chen, and G. J. Cheng, *ACS Nano* **9**, 10018 (2015).

- ¹⁶Y. Liu, F. Wang, J. Zhao, L. Jiang, M. Kiguchi, and K. Murakoshi, *Phys. Chem. Chem. Phys.* **11**, 6514 (2009).
- ¹⁷D. Wang, J. Zhao, S. Hu, Y. Xing, S. Liang, Y. Liu, and S. Deng, *Nano Lett.* **7**, 1208 (2007).
- ¹⁸B. Wang and G. Wang, *Opt. Lett.* **29**, 1992 (2004).
- ¹⁹T. A. Rajesh and D. Kumar, *Sensor. Actuat. B-Chem.* **136**, 275 (2009).
- ²⁰A. Javey, J. Guo, Q. Wang, M. Lundstrom, and H. Dai, *Nature* **424**, 654 (2003).
- ²¹A. H. Flood, J. F. Stoddart, D. W. Steuerman, and J. R. Heath, *Science* **306**, 2055 (2004).
- ²²J. Yeo, G. Kim, S. Hong, J. Lee, J. Kwon, H. Lee, H. Park, W. Manokrotul, M. T. Lee, B. J. Lee, C. P. Grigoropoulos, and S. H. Ko, *Small* **10**, 5015 (2014).
- ²³D. E. Johnston, D. R. Strachan, and A. T. C. Johnson, *Nano Lett.* **7**, 2774 (2007).
- ²⁴J. M. Baik, S. J. Lee, and M. Moskovits, *Nano Lett.* **9**, 672 (2009).
- ²⁵J. Zhao, H. Sun, S. Dai, Y. Wang, and J. Zhu, *Nano Lett.* **11**, 4647 (2011).
- ²⁶J. M. Campbell and R. G. Knobel, *App. Phys. Lett.* **102**, 023105 (2013).
- ²⁷M. L. Perrin, C. J. O. Verzijl, C. A. Martin, A. J. Shaikh, R. Eelkema, J. H. van Esch, J. M. van Ruitenbeek, J. M. Thijssen¹, H. S. J. van der Zant, and D. Dulic, *Nat. Nanotechnol.* **8**, 282 (2013).
- ²⁸C. A. Martin, R. H. M. Smit, H. S. J. van der Zant, and J. M. van Ruitenbeek, *Nano Lett.* **9**, 2940 (2009).
- ²⁹A. R. Champagne, A. N. Pasupathy, and D. C. Ralph, *Nano Lett.* **5**, 305 (2005).
- ³⁰K. Liu, P. Avouris, J. Bucchignano, R. Martel, S. Sun, and J. Michl, *Appl. Phys. Lett.* **80**, 865 (2002).
- ³¹A. Cui, Z. Liu, H. Dong, Y. Wang, Y. Zhen, W. Li, J. Li, C. Gu, and W. Hu, *Adv. Mater.* **27**, 3002 (2015).
- ³²S. Karim, M. E. Toimil-Molares, A. G. Balogh, W. Ensinger, T. W. Cornelius, E. U. Khan, and R. Neumann, *Nanotechnology* **17**, 5954 (2006).
- ³³S. Hong, J. Yeo, J. Lee, H. Lee, P. Lee, S. S. Lee, and S. H. Ko, *J. Nanosci. Nanotechnol.* **15**, 2317 (2015).
- ³⁴J. Lee, P. Lee, H. Lee, D. Lee, S. S. Lee, and S. H. Ko, *Nanoscale* **4**, 6408 (2012).
- ³⁵S. Han, S. Hong, J. Yeo, D. Kim, B. Kang, M. Y. Yang, and S. H. Ko, *Adv. Mater.* **27**, 6397 (2015).
- ³⁶P. Lee, J. Lee, H. Lee, J. Yeo, S. Hong, K. H. Nam, D. Lee, S. S. Lee, and S. H. Ko, *Adv. Mater.* **24**, 3326 (2012).
- ³⁷S. J. Henley, M. Cann, I. Jurewicz, A. Dalton, and D. Milne, *Nanoscale* **6**, 946 (2014).
- ³⁸J. A. Spechler, K. A. Nagamatsu, J. C. Sturm, and C. B. Arnold, *ACS Appl. Mater. Interfaces* **7**, 10556 (2015).
- ³⁹P. Peng, A. Hu, A. Gerlich, G. Zou, L. Liu, and Y. N. Zhou, *ACS Appl. Mater. Interfaces* **7**, 12597 (2015).
- ⁴⁰S. Dai, Q. Li, G. Liu, H. Yang, Y. Yang, D. Zhao, W. Wang, and M. Qiu, *Appl. Phys. Lett.* **108**, 121103 (2016).
- ⁴¹J. Lee, J. Y. Woo, J. T. Kim, B. Y. Lee, and C. S. Han, *ACS Appl. Mater. Interfaces* **6**, 10974 (2014).
- ⁴²L. Lin, G. Zou, L. Liu, W. W. Duley, and Y. N. Zhou, *Appl. Phys. Lett.* **108**, 203107 (2016).
- ⁴³W. H. Chung, S. H. Kim, and H. S. Kim, *Sci. Rep.* **6**, 32086 (2016).
- ⁴⁴X. Chen, Y. Chen, M. Yan, and M. Qiu, *ACS Nano* **6**, 2550 (2012).
- ⁴⁵Z. Guo, Y. Zhang, Y. DuanMu, L. Xu, S. Xie, and N. Gu, *Colloids Surf., A* **278**, 33 (2006).
- ⁴⁶Y. Wen, Q. Zhang, J. Zheng, Z. Zhu, and S. Sun, *J. Phys. Chem. C* **113**, 20611 (2009).